JOURNAL OF MATERIALS SCIENCE 26 (1991) 6151–6160

Three-dimensional optical microscopy of water trees in polyethylene

D. M. SHINOZAKI
Department of Materials Engineering, University of Western Ontario, London, Ontario, Canada N6A 5B9

P. C. CHENG
Advanced Microscopy and Imaging Laboratory, Department of Electrical and Computer Engineering, State University of New York, Buffalo, NY 14260, USA

S. HARIDOSS
AT Plastics Inc., Brampton, Ontario, Canada L6W 3G4

R. MITCHELL, A. FENSTER
Imaging Research Laboratories, The J. P. Robarts Research Institute, London, Ontario, Canada N6A 5K8

Polyethylene is used as high-voltage electrical insulation in cable, and fails when subjected to the combination of water environment and electrical field. The three-dimensional microstructure of water trees, which are precursors to dielectric breakdown, has been revealed with laser scanning confocal optical microscopy. Two-dimensional images which represented optical serial sections were recorded in digital form, and reconstructed in a computer to produce three-dimensional views of the microstructure. Both stereo pairs and computed tomographic reconstructions were made. The material was stained with a fluorescent dye and the fluorescent image was compared to the standard unstained image. The dye was found to increase the signal-to-noise ratio and improve the quality of the image significantly.

1. Introduction

The microstructure of polymers can be examined using a variety of methods. Techniques which involve ionizing radiation such as electron microscopy produce artefacts in the image which are a result of the radiation damage in the polymer, and which limit the minimum resolvable structure to approximately 20 nm for polyethylene [1]. Standard optical microscopy can be used to resolve detail which is somewhat more than one order of magnitude larger. The usefulness of optical microscopy in the examination of polymers is derived from the absence of ionizing radiation damage artefacts, because the photon energies are too small to produce ionization in the material, and in the minimal specimen preparation necessary in many cases.

The resolution of conventional optical microscopy is determined by the wavelength of the light, the numerical aperture of the lens, and the signal-to-noise level in the image. Two points in the specimen produce two Airy discs in the image plane, which can be distinguished as separate structures provided the Rayleigh criterion is satisfied

$$d = 1.22 \frac{\lambda_0}{NA_{\text{objective}} + NA_{\text{condenser}}} \quad (1)$$

where $NA_{\text{objective}}$ and $NA_{\text{condenser}}$ are the numerical apertures of the objective and condenser lenses, and d is the minimum resolvable separation of two points in the specimen.

Conventional optical microscopy is used to examine polymers in both reflected and transmitted light modes. In transmitted light microscopy, thin specimens are used, which typically have a thickness between 1 and 40 μm. The observation of small structures, approaching the limit of resolution, requires that the signal-to-noise ratio be appropriately high. In attempting to resolve small structures in a thick specimen, the signal-to-noise ratio is very small, because the incident light is scattered from volume elements in the specimen which lie above and below the focal plane of interest. This background scatter reduces the visibility of the structure of interest.

In reflected light mode, the same problem arises, even in examining the near surface regions, because the light which is scattered diffusely from structures above and below the plane being examined increases the background noise in the image.

In polymers such as polyethylene, the material is inherently quite transparent to visible light, and it would very useful to be able to examine small structures deep within the specimen without sectioning exactly to the plane of interest. Confocal optical microscopy offers this possibility and this work illustrates the application of this relatively novel method to the problem of water trees in polyethylene.

0022–2461/91 $03.00 + .12

1.1. Confocal optical microscopy

Confocal optical microscopy has been described in a number of papers in the biological microscopy literature [2, 3]. In the study of the microstructure of biological materials, the recording of three-dimensional optical images is possible because the materials are often quite transparent. This also holds for many synthetic polymers such as polyethylene.

The particular advantages of confocal microscopy in obtaining three-dimensional images can be understood by considering the general principles of the method (Fig. 1). The schematic diagram shows a typical configuration for confocal microscopy in a reflected light mode, in which the light source and signal detector lie on the same side of the specimen. The arrangement for fluorescent microscopy is similar although the signal from the specimen comes from fluorescence of the microstructure rather than reflection.

The incident light source is a laser which illuminates a pinhole. The image of the source pinhole is focused to the focal plane on the objective lens in the specimen. Light is scattered from the various microstructural elements in the specimen which lie at any point along the incident light path. However, the light reflected from the focal plane in the specimen will follow an optical path back through the source pinhole. Because the detector and laser cannot occupy the same position, the source and detector pinholes are spatially separate, with a beam splitter between them. The exit pinhole is placed in the conjugate position with respect to the source pinhole. Light which is scattered by microstructural elements which lie above or below the exact focal plane does not pass through the detector pinhole (broken lines representing the reflected light rays). The signal which is detected therefore emanates mainly from the exact focal plane. The incident light can be moved over the specimen in a rectangular raster pattern, and the reflected signal recorded point by point to produce the image of the microstructure (alternatively, the specimen can be moved).

A series of images can be so recorded at different depths in the specimen by changing the focal plane position (by moving the specimen stage) (Fig. 2). These images can then be computer processed to present the information as a stereo pair or as a more complete three-dimensional reconstruction (Section 2.4).

One of the main advantages of confocal microscopy is that a minimum amount of specimen preparation is needed. An alternative, comparable microstructural study would involve microtoming a series of thin sections from the specimen, and recording an image from each section, ensuring that the successive images are recorded in accurate registration with each other.

The specimen for confocal microscopy requires little, if any special preparation provided the surface is clean and reasonably flat. The serial images are recorded digitally, and the time to record 50–100 images which are typically taken over a depth of 50–200 μm may be of order of tens of minutes. Because the images are recorded in sequence without moving the specimen laterally, the slice-to-slice registration is accurately maintained.

The resolution of confocal microscopy must be considered in three dimensions: parallel to the optical axis, and in the focal plane of the objective lens. The depth resolution depends on a number of factors, including the numerical aperture of the objective lens,

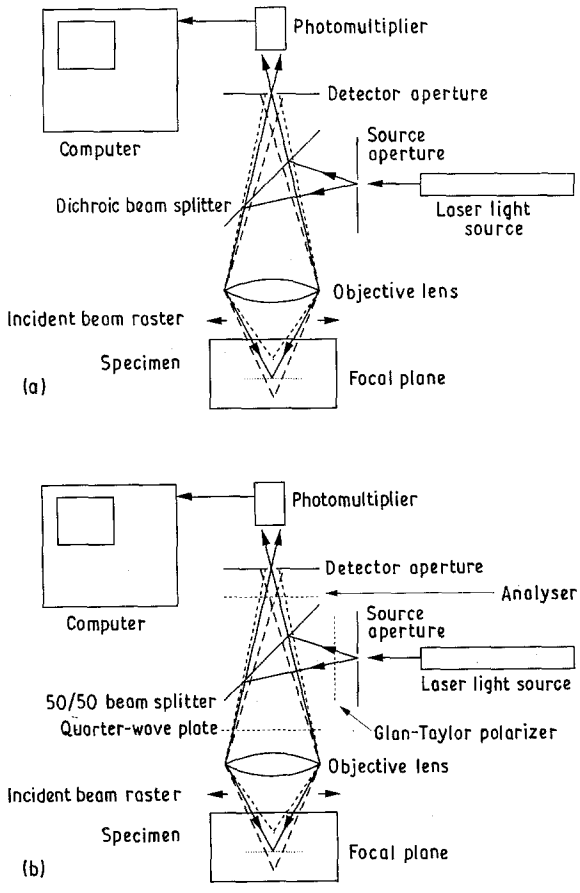

Figure 1 (a) Schematic diagram of a laser scanning confocal microscope arrangement to obtain fluorescent images. (b) Insertion of polarizer, analyser and quarter-wave plate to remove internal reflections which obscure the image when the instrument is used in reflected or backscattered modes.

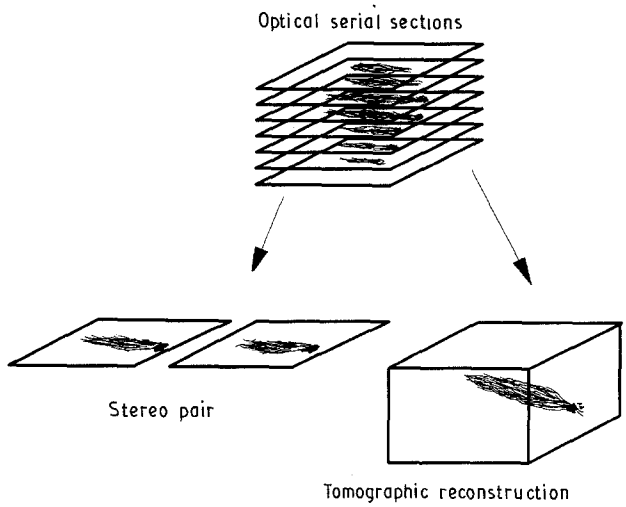

Figure 2 Optical serial sections obtained from confocal microscopy reconstructed into a stereo pair or into a complete tomographic image.

the wavelength of the radiation, and the pinhole diameter [4]. The optical sectioning strength, which is the rate at which measured signal intensity decreases with distance parallel to the optical axis, can be optimized, and experimentally, the axial resolution of the confocal microscope is considerably better than 1 μm.

The resolution in the focal plane depends on the spot size which can be described in terms of the Rayleigh criterion (Equation 1). However, in the confocal case, the illuminated area in the spot can be limited by the aperture, and the achievable resolution is significantly better, the smallest resolvable structure being about 1.4 times smaller than that visible in a normal optical microscope [4].

The high resolution which can be achieved with confocal microscopy makes the method applicable for a wide variety of microstructural studies in materials. The examination of three-dimensional sub-micrometre dimensioned structures in polymers and composites without special specimen preparation is potentially extremely useful. The recent availability of powerful microcomputers and the associated reconstruction algorithms makes it straightforward to obtain a three-dimensional image. The present work is an illustration of the application of these methods to the study of water trees.

1.2. Water trees in polyethylene

A typical high-voltage power cable (Fig. 3) consists of concentric layers of (a) metallic conductor, (b) conductor shield (carbon black-filled cross-linkable ethylene copolymer, often described as a semi-conductive layer), (c) cross-linked polyethylene insulation, (d) insulation shield (similar to conductor shield, (e) wire or metallic tape, and sometimes (f) a jacket. The purpose of the conductor shield is to minimize the strand effect, to prevent ionization of air at the surface of the conductor. It should adhere well to the conductor and polyethylene insulation, whereas the insulation shield must separate easily for subsequent joining processes during installation of the cable.

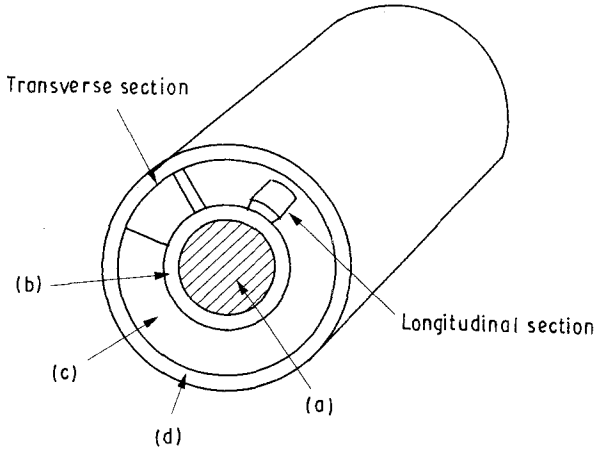

Figure 3 High-voltage cable: (a) metallic conductor, (b) conductor shield, (c) cross-linked polyethylene insulation, (d) insulation shield. The electric field is oriented in the radial direction, and the water trees grow parallel to the field.

In service, high-voltage cables which are exposed to water can degrade slowly; the dielectric strength of the polyethylene insulation decreases to a point where complete electrical breakdown occurs. The mechanism by which the polyethylene degrades involves the nucleation and growth of water trees, which consist of microcavities filled with water. The water trees can grow to dimensions of 10–500 μm long (oriented parallel to the electric field). The catastrophic electrical breakdown of the insulator occurs at one of the many water trees.

The study of the nucleation and growth processes of water trees is therefore an essential part of controlling such electrical failures in cable. It is important to characterize the morphology of the trees, the distribution of the microcavities, and the relationship of the tree to the nucleation event. The tree can originate inside the insulation usually from a cavity, imperfection or contaminant and grow in the field direction and is called a "bow-tie" tree, or it can initiate at the insulation–semiconductive interface and is known as a "vented tree".

There is an extensive literature on some aspects of the microstructure of water trees [5]. In the present work, a method for examining the three-dimensional morphology of the trees is reported. Specimen preparation artefacts which can distort the surfaces or the thin films used in two-dimensional studies have been eliminated by using the optical sectioning capability of confocal optical microscopy.

2. Experimental procedure

2.1. Samples

Two different samples were used for the present investigation: (1) 5–35 kV rated XLPE insulated cable samples after accelerated laboratory ageing, (2) 15 kV XLPE insulated cable samples removed from the field after failure.

The cable material was sectioned with a steel blade in two perpendicular sections (Fig. 3). The electric field was oriented in the radial direction, so the water trees were macroscopically oriented in this direction. The longitudinal section therefore cut across the tree, while the transverse section cut parallel to the trees.

2.2. Confocal microscope

In these experiments, a modified BioRad MRC500 laser scanning confocal microscope was used in both reflected and epifluorescent mode. The 488 nm emission line of a 25 mW argon ion laser was used as a light source. The BioRad BHS green filter was used in these experiments. This consists of a dichroic beam splitter (Omega DR510LP), and a barrier filter (Omega OG515) which allowed a green fluorescent image to be recorded. Four of the aluminium-coated folding mirrors in the original BioRad microscope were replaced with high-reflectivity dielectric mirrors to increase the detected signal. In order to eliminate the internal reflection from optical elements within the microscope, the instrument has been further modified.

A Glan-Tayler type polarizer (a double calcite prism) was placed in the illuminating laser beam to achieve high polarization extinction for the illuminating beam, and a quarter-wave retardation plate was inserted in the optical path just above the objective to change the linearly polarized illuminating beam to a circularly polarized form. An analyser is placed just in front of the detector. This arrangement removes most of the unwanted reflection from the microscope lens elements [6].

2.3. Fluorescent staining of water trees

For the particular example in this work, the optical difference (absorption, refraction and scattering) between the volume in the water tree and the matrix material is small, and normally the water tree is not easily distinguishable from the matrix. The specimens were therefore "stained" in a fluorescent medium. The dye in this case filled the microcavities of the water trees.

At the limit of lateral and axial resolution, the volume element in the specimen from which the signal emanates is very small, and the total signal can be low. By staining the specimen so that the microstructure differentially takes up the fluorescent dye, the difference in signal from stained and unstained regions of the microstructure can be increased. The image contrast in this case is related to the ratio of the fluorescent signal from the water tree and from the background. The contrast for a stained material is therefore increased compared to an unstained material. In these experiments, cable slices were cut with a steel blade and stained with a solution of 0.1% 5-fluorescein iso-thiocyanate (FITC) in ethanol for 30 min at 50 °C. The FITC dye has an excitation wavelength in the blue range of light and a fluorescent emission in the green. The dye is commonly used in biology for tagging protein molecules.

In order to achieve optimum optical performance, the cable slice was mounted in immersion oil (with an index of refraction of 1.53) in between a microscope slide and cover glass. For minimum section thickness and maximum signal strength, an oil immersion high-numerical objective (Nikor Fluor 40 ×, NA = 1.4) was used in this study.

Optically sectioned images were recorded at different depths in the specimen as described in Section 1.1. The images were acquired at a rate of 1 frame/second with a Kalman signal filter. They were stored digitally using a Synopics image processing board installed on an 80286 AT-bus microcomputer in an 8 bit 768 × 512 format. The multiple slice images, each of which required 384 kbytes, were stored on a 320 Mbyte hard disk and later transferred to tape. For tomographical reconstruction, the serial images were analysed on a workstation described in Section 2.4.

2.4. Digital reconstruction of the three-dimensional image

The series of two-dimensional images were subsequently processed to present three-dimensional information about the structure. The image can be presented in a number of different ways, depending on the computer algorithms used. A simple stereo pair can be shown, in which the images from successive layers are superimposed with proper lateral shifting of the successive images. However, a more complete picture of the three-dimensional information is found in the tomographic reconstruction of the data set. The representation of the three-dimensional information is important in the final interpretation of the image, and it is useful to distinguish at this point between the various methods available.

In three dimensions the image is represented by volume elements (voxels), each with a specified intensity. The interpretation of the image depends on the

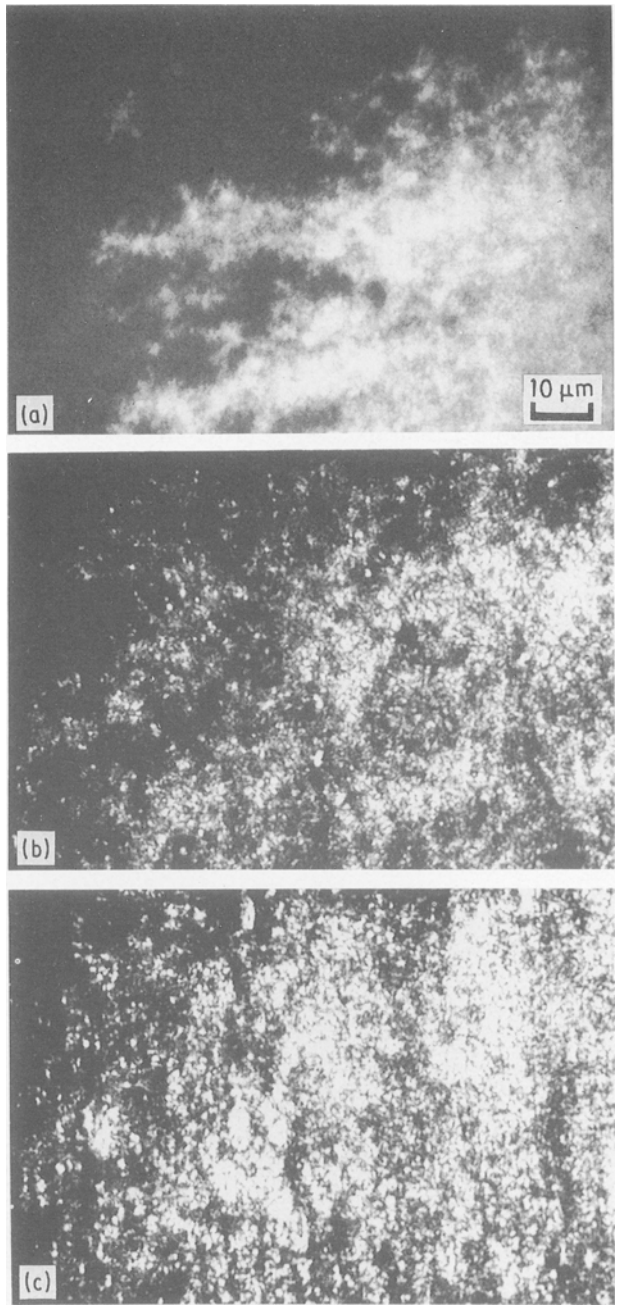

Figure 4 Longitudinal section from the polyethylene insulation, viewed parallel to the water trees along the electric field direction. Two similar trees are shown: (a) unstained, and (b, c) two optical sections from one tree, stained with fluorescent dye (FITC).

way the information is presented [7]. For many applications this is reduced to the problem of representing or rendering the three-dimensional data on a two-dimensional display. Three general techniques are used: contours, surface rendering, and volume rendering. Contours and surface rendering are useful for some applications, and have been discussed previously [7–13].

Volume rendering techniques reformat a series of two-dimensional slices into a three-dimensional volume. Often, new slices are interpolated between existing ones so that the voxel regions are more closely cubical. After the reformatted three-dimensional volume is constructed, a number of rendering techniques may be used for display. One of the simplest is multi-planar reconstruction (MPR) [14]. With this method an

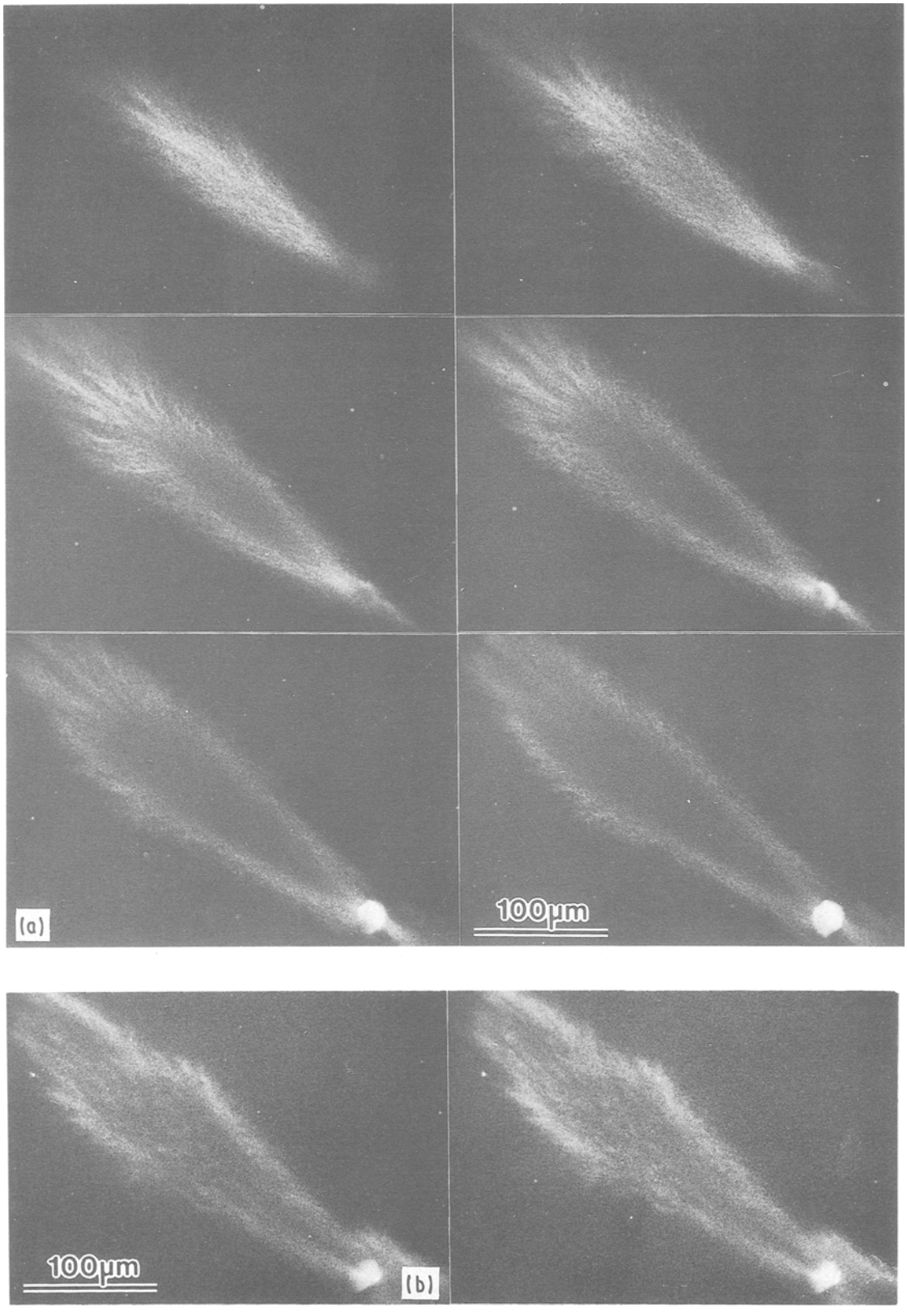

Figure 5 (a) Low-magnification optical sections of one-half of a "bow-tie" water tree. The images are taken at 10 μm steps. (b) Stereo pair reconstructed from the serial sections shown in (a).

arbitrary plane is specified inside the three-dimensional volume. Data along this plane are interpolated from existing voxels, extracted and displayed. Many imaging workstations are capable of performing this reconstruction in real time [8] and combining it with other rendering techniques described below.

The other volume rendering algorithms generally consider each voxel in the reformatted volume every time an image is created. These algorithms can be classified into two general categories, those that are driven by the voxels in the volume, and those that are driven by the pixels in the output image. Algorithms driven by voxels in the volume process those voxels in either a back-to-front (BTF), or a front-to-back (FTB) order [15].

The BTF algorithm uses a user-specified viewing position to determine a viewing plane perpendicular to the line connecting the viewing position and the centre of the voxel volume. Then the voxels in the volume are "read out" and projected on to pixels in the viewing plane, starting at the "back" or furthest corner of the object. With this technique, hidden surface elimination is taken care of implicitly, as voxels closer to the view plane "overwrite" those behind them.

The FTB algorithm is similar, except that voxels are read out starting at the nearest corner of the volume. With this approach, once a pixel in the viewing plane is written into, it may not be overwritten thus obstructed surfaces are never displayed. Typically only half of the voxel volume need be read out before the viewing plane is full. Therefore, this algorithm is computationally more efficient than BTF.

However, both algorithms have the problem that a single voxel in the volume may correspond to more than one pixel in the viewing plane. The area overlap of the voxel on pixels in the viewing plane has to be calculated. This compromises the bulk of the computational effort.

The second general category of volume rendering algorithms, those driven by the pixels in the viewing plane, are known as ray casting algorithms. With this approach, each pixel in the viewing plane is the source of one or more "rays" which are projected towards the voxel volume. Data values at any point along each ray are determined by interpolating from surrounding

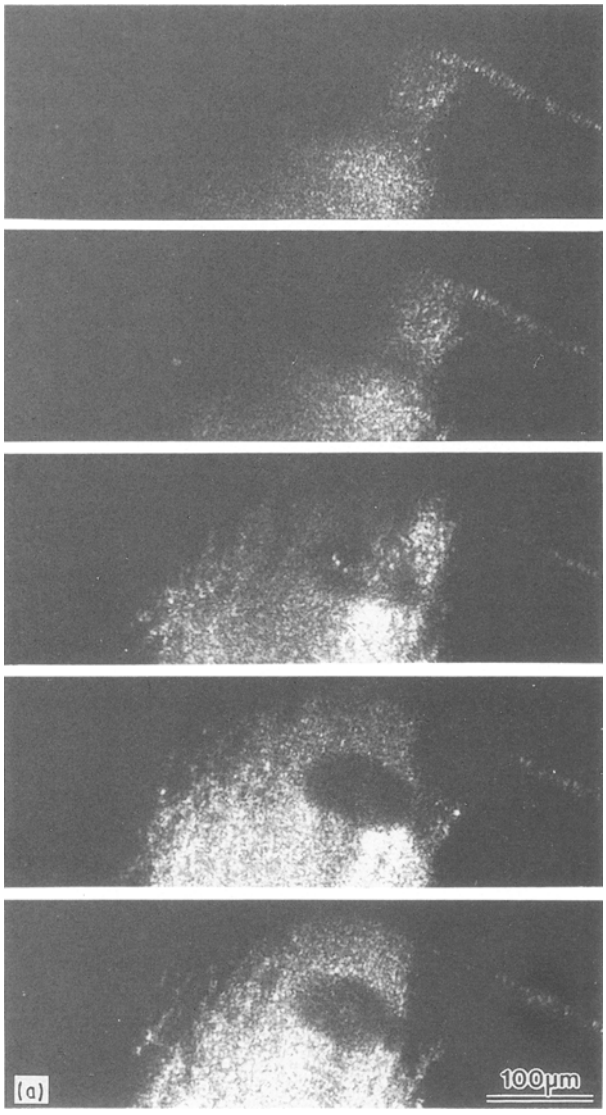

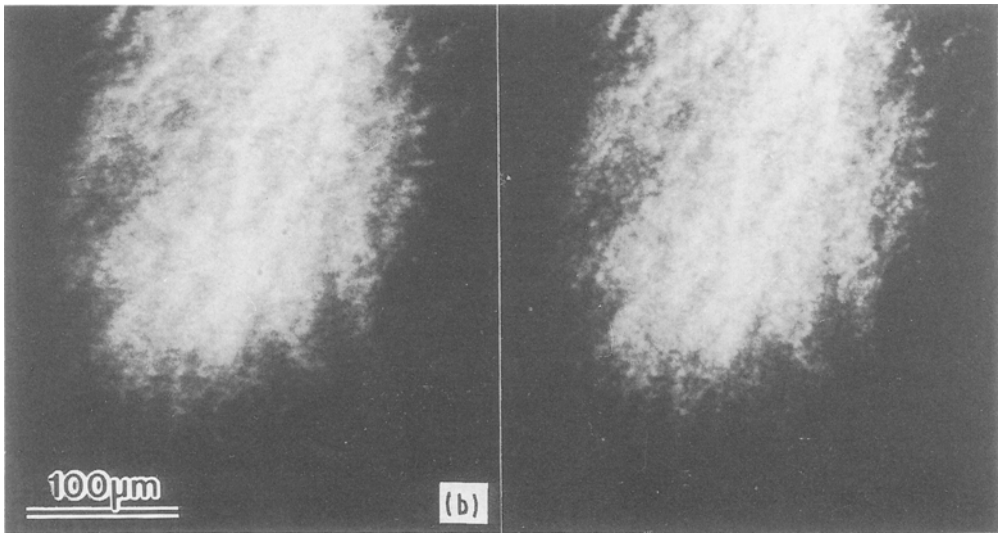

Figure 6 (a) Vented water tree initiating near the interface at "I" between the polyethylene insulation (lower portion of the image) and the semi-conductive shield. (b) Stereo pair of the growing end of the tree shown in (a). The inhomogeneity of the structure is visible.

voxels. A number of interpolation schemes are available including nearest neighbour, trilinear and cubic spline [8]. Nearest neighbour is easy to implement and computationally cheap, but may lead to aliasing in the output. Trilinear interpolation (used in the present work) is slightly more difficult to implement, reasonably inexpensive computationally, and gives results which are usually better than nearest neighbour. Spline interpolation is the most difficult of the three to implement, and the most expensive. However, it can give results significantly better than the other two.

As data values along the ray are determined, a number of options are available. Surfaces can be defined which cover ranges of data values. When projected rays intersect a surface various shading models may be used to render it [10]. A surface may also have characteristics such as opacity and colour associated with it. In this case, the colour of the source pixel in the viewing plane is a weighted product of the opacity of the surface and its colour. If the surface is partially transparent, the ray may carry on (with possible reflections and refractions) to intersect further surfaces which, in turn, contribute to the source pixel colour. Alternatively, the distance from the source pixel to the destination surface may be recorded in the source pixel, then some local gradient operation is applied to the viewing plane to produce the shaded image. There are a number of alternatives [16]. Yet another technique is simply to sum, in the source pixel, all data values along the ray. The resulting image is similar in nature to a conventional radiograph [7]. In general, volume rendering techniques are slow but produce very high quality images which can approach photo-realism.

Regardless of the rendering technique used, multiple images of the same volume can be created by rotating the volume slightly, and repeating the rendering process. When these images are played back in quick succession a "movie" of the object rotating in space results. The additional depth cues added by even slight rotation are often sufficient to reveal considerable structural information [8].

For the present work, the two-dimensional confocal images described in Section 2.3 were reformatted into a three-dimensional array with dimensions $400 \times 400 \times 26$, for display on a Sun Microsystems 4/260 workstation with a TAAC-1 accelerator. The TAAC-1 interpolated additional slices in the volume to obtain an array with dimensions $400 \times 400 \times 200$. The "Voxvu" rendering software provided with the TAAC-1 allows real time MPR. A ray casting mode is also available to generate synthetic "radiographic-type" image, which is similar to an X-ray image, although in this case optical rays are used; or to render surfaces corresponding to distinct ranges of data values. Users can specify up to eight surfaces each having a particular opacity and colour [17]. This software was used to generate rotating synthetic "radiographic-type" movies of the water tree. For presentation in this paper, selected individual frames from this movie are shown in sequence. The time required to generate a single frame in this movie was approximately 5 min. 60 frames were produced each rotated 3° about the volume to give a continuous smooth motion when played back. The three-dimensional interpretation is therefore very clear in the movie version of the tomographic reconstruction.

3. Results and discussion

The specimen preparation included staining with a fluorescent dye. The advantage of this is seen in Fig. 4. Similar water trees with and without FITC stain are shown. The diffuse, poorly differentiated images without staining contrast with the clearly defined images of the stained samples. The smallest cavities seen here are less than 1 μm, and are much more easily seen in the stained sections. The images were taken from a longitudinal section of the cable (Fig. 3), and the viewing direction is parallel to the field (normal to the images seen in Fig. 6, for example). In the stained images the clustering of the microcavities is visible as patchiness on the scale of 10 μm or more. The last two images are a pair taken from the same tree at different depths. The

Figure 7 Stereo pair of a filament between two water trees, illustrating the discontinuity of the microcavities.

change in the microcavity distribution as function of position along the tree is clear.

A typical large "bow-tie" water tree is shown in Fig. 5a. Only half the "bow-tie" is shown. The point of origin in this kind of tree is in the central defect which shows as a bright area in the lower right corner. The images were taken at low magnification, at different depths with intervals of 10 μm between steps. Large areas can be examined, and gross morphological features easily delineated.

The stereo pair images of this water tree are given in Fig. 5b. These images are reconstructed from the optical serial sections by superimposing the optical serial sections on the computer screen with each successive section being shifted by an integer number of pixels. This creates an artificial parallax so the two resultant images appear to be views from different orientations [18].

Water from surroundings is found to have drawn to the tips of this water tree. This is the most classical

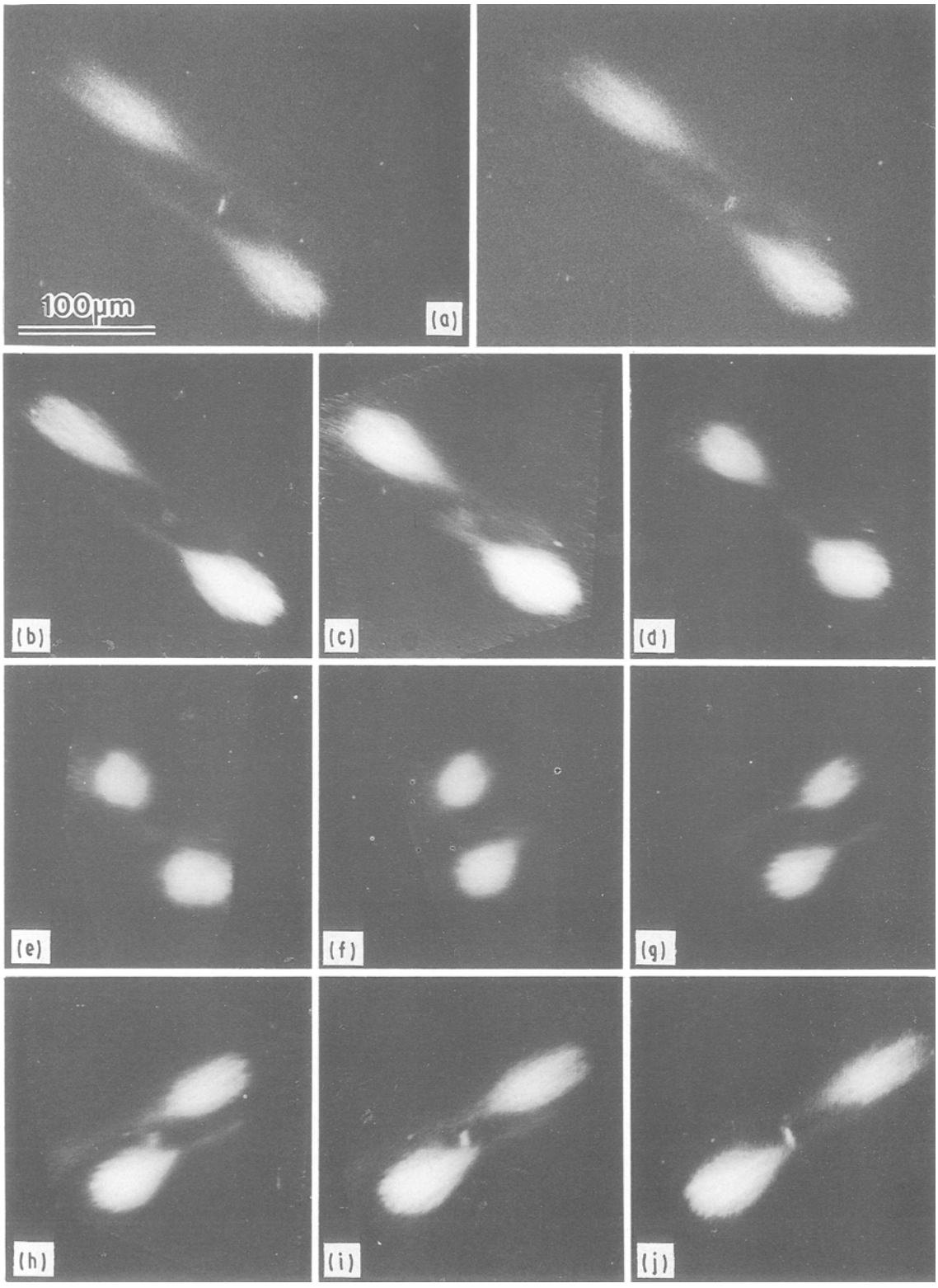

Figure 8 Tomographic reconstruction of a "bow-tie" water tree. (a) is a stereo pair from the same data set as (b–j).

example for which the electric field distribution can be arrived at analytically assuming an ellipsoid of dielectric constant $E = 10$ in polyethylene [19].

Fig. 6a shows the image of a vented tree initiating from the interface between semiconductive and insulation. A particle which is darker than the rest of the water tree is associated with the region near the interface. This darker region emits a lower fluorescent signal and hence has a lower microcavity density. The region is centred about 4 μm from the outside surface of the tree. At high magnification, with a focusing step size of 1 μm, the void morphology at the point of origin can be compared to that at the leading boundary of the tree, furthest away from the point of origin (Fig. 6b). Because the void diameter is of the order of 1 μm and the optical sections are taken at 1 μm intervals, the contiguity of the voids can be examined. If particular voids are identified and followed from layer to layer, it can be seen that voids are not joined. The void size is also similar at the point of origin and at the growth boundary. Several observations confirm the discontiguous nature of microvoids constituting water trees [20].

The boundary between the polyethylene insulator and the semi-conductive layer is brighter than the background, indicating a region into which the stain can diffuse easily. This in itself may be significant because the boundary is therefore a region of high diffusivity.

The non-contiguous nature of the microcavities is more clearly illustrated in the stereo pair of Fig. 7. A filament has formed between two arms of a mature water tree, and the serial sections reveal the discrete microcavities which constitute a seemingly continuous filament. The three-dimensional view revealed in the stereo pair shows a discontinuous, meandering filament. In terms of the formation of these filaments or microchannels the stresses generated by the high fields clearly mucleate microcavities slightly ahead of the growing front, and the water which fills these cavities must diffuse through the polyethylene. The local diffusion processes within the polyethylene must clearly be affected by the lamellar microstructure within these regions. The opening of microcavities under the influence of the diffusing water and high electrical fields is essentially a deformation process similar to that observed during tensile testing of polymers [21]. It is likely, based on observations made in deformation studies, that the localized microcracking initiates in the interlamellar regions, and the progression of the filaments follows some interlamellar paths. Such filaments or microchannels could act as initiation sites for electrical trees leading to the dielectric breakdown.

The three-dimensional reconstruction of a bow-tie tree is shown in Fig. 8. A stereo pair is shown in Fig. 8a while the full three-dimensional reconstruction using a ray casting algorithm described in Section 2.4 is shown in the bottom nine images (Fig. 8b–j). The

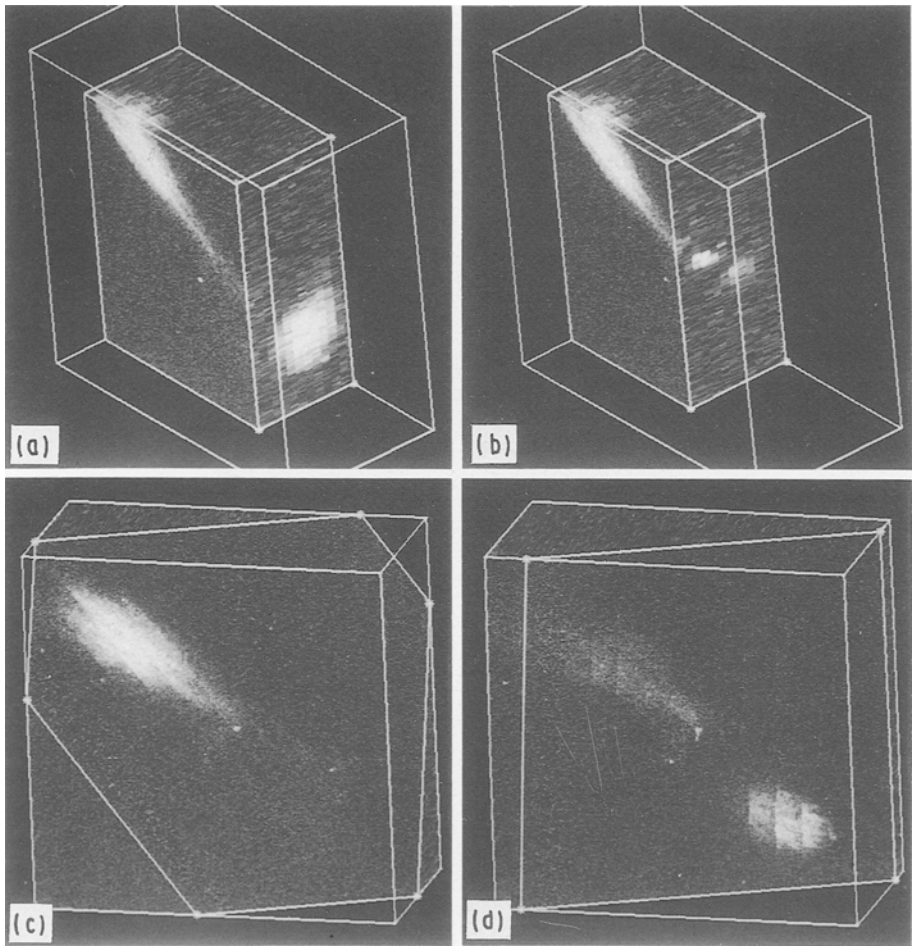

Figure 9 Examples of arbitrary optical sections which can be viewed from the data set of Fig. 8.

same confocal optical sections were used to reconstruct both the stereo pair and the tomographic views. Each image in the tomographic series represents a view which is rotated in 18° steps. The overall shape is clearly seen, and the trees which are elongated in the field direction are not collinear with the central point of origin. The additional morphological information in a full tomographic reconstruction is evident by comparison with the stereo pair above. The image is progressively rotated to reveal the true overall morphology of the water tree and its relationship to the defect at which it is initiated.

An important application of the full three-dimensional reconstruction is shown in Fig. 9. Arbitrary viewing sections can be cut in any orientation to reveal microstructure on specific planes. Fig. 9a and b show viewing boxes with sides parallel to the overall box, while Fig. 9c and d show two oblique planes cutting the water tree at arbitrary sections. The sectioning mode of examination of the three-dimensional morphology is rapid once the three-dimensional reconstruction has been completed.

The section shown in Fig. 9d shows the original optical section planes, and illustrates one source of misinterpretation in such images. For serial sections taken in coarse steps, the information between planes is interpolated, and unless taken into account, can lead to an incorrect interpretation of the microstructure. In this example, coarse steps were used to emphasize the effect.

4. Conclusions

The use of confocal optical microscopy to examine water trees in polyethylene cable insulation has been demonstrated. The high resolution available in the technique reveals uniform size distribution of voids throughout a given tree. However, the fluorescent dye is inhomogeneously distributed in the tree, suggesting the diffusion paths for the liquid is easier in some regions. The confocal images represent an optical serial sectioning method which is rapid and requires only minimal specimen preparation. The three-dimensional images which can be easily constructed from the optical serial sections using well-established computer methods, are useful in delineating the exact morphology of the tree and its relationship to the initiating defect.

Acknowledgements

The work was supported by NSERC (Canada); grants from the US DOE (DE-AE-08-88DP10782 and EE-FG03-89SF18012); the Whitaker Foundation Biomedical Engineering Program; CAT-HIDI and NFWWTP.

References

1. L. C. SAWYER and D. T. GRUBB, "Polymer Microscopy" (Chapman and Hall, London, 1987).
2. S. INOUE, in "The Handbook of Biological Confocal Microscopy", edited by J. Pawley (IMR Press, Wisconsin, 1989) p. 1.
3. J. G. WHITE, W. B. AMOS and F. FORDHAM, *J. Cell Biol.* **105** (1987) 41.
4. T. WILSON, in "The Handbook of Biological Confocal Microscopy", edited by J. Pawley (IMR Press, Wisconsin, 1989) p. 99.
5. M. T. SHAW and S. H. SHAW, *IEEE Trans. EI* **19** (1984) 419.
6. P. C. CHENG and R. G. SUMMERS, in "The Handbook of Biological Confocal Microscopy", edited by J. Pawley (IMR Press, Wisconsin, 1990) p. 163.
7. E. BUHLE, P. SMITH and U. ABEI, in "Proceedings of the IEEE First Conference on Visualization in Biomedical Computing" (IEEE Computer Society Press, Los Alamitos, CA, 1990) p. 66.
8. S. GOLDWASSER, R. REYNOLDS, D. TALTON and E. WALSH, *Comp. Med. Imag. Graphics* **12** (1) (1988) 1.
9. J. K. UDUPA, *Proc. IEEE* **71** (1983) 420.
10. J. FOLEY and A. VAN DAM, "Fundamentals of Interactive Computer Graphics" (Addison-Wesley, Reading, MA, 1982).
11. W. LORENSEN and H. CLINE, *Computer Graphics* **21** (4) (1987) 163.
12. R. S. ACHARYA, P. C. CHENG, J. SAMARABANDU, L. H. CHEN, R. G. SUMMERS and C. E. MUSIAL, *Trans. R. Microsc. Soc.* (1990) **1** (1990) 289.
13. R. G. SUMMERS, C. E. MUSIAL, P. C. CHENG, A. LEITH and M. MARKO, *J. Electron Microscop. Technique* (1990) in press.
14. S. ROTHMAN, G. DOBBEN, M. RHODES, W. GLENN and Y. AZZAWI, *Radiology* **150** (1984) 185.
15. R. REYNOLDS, D. GORDON and L. CHEN, *Comput. Vision Graph. Image Process.* **38** (1987) 275.
16. L. CHEN, G. HERMAN, R. REYNOLDS and J. UDUPA, *IEEE Comput. Graph. Applic.* **5** (12) (1985) 33.
17. D. McMILLAN, R. JOHNSON and C. MOSHER, *SunTech J.* **2** (4) (1989) 52.
18. A. BOYD, in "The Handbook of Biological Confocal Microscopy", edited by J. Pawley (IMR Press, Wisconsin, 1990) p. 163.
19. P. PATCH, A. PASIMADAKIS and P. ROMERO, in "IEEE International Symposium EI", June 1990, Toronto, Canada (IEEE Dielectrics and EI Society Press, 1990) p. 160.
20. S. BAMJI, A. BULINSKI, J. DENSLEY and A. GARTON, *IEEE Trans EI* **18** (1983) 32.
21. F. ZOK and D. M. SHINOZAKI, *J. Mater. Sci.* **22** (1987) 3995.

Received 24 August 1990
and accepted 28 February 1991